

Likelihood Non-Gaussianity in Large Scale Structure Analyses

ChangHoon Hahn, et al.

Lawrence Berkeley National Laboratory, 1 Cyclotron Rd, Berkeley CA 94720, USA

`changhoon.hahn@lbl.gov`

DRAFT --- 690c3be --- 2018-01-01 --- NOT READY FOR DISTRIBUTION

ABSTRACT

Standard present day large-scale structure (LSS) analyses make a major assumption in their Bayesian parameter inference — the likelihood has a Gaussian functional-form. We investigate the impact of this assumption on two recent LSS analyses: the [Beutler et al. \(2017\)](#) powerspectrum multipole (P_ℓ) analysis and the [Sinha et al. \(2017\)](#) group multiplicity function (ζ) analysis. Using non-parametric divergence estimators on mock catalogs originally constructed for covariance matrix estimation in these analyses, we identify significant non-Gaussianity for both P_ℓ and ζ likelihoods. Afterwards, we use Gaussian mixture density estimation and Independent Component Analysis to construct likelihood estimates that better approximate the true likelihood than the Gaussian *pseudo*-likelihood. We then use the likelihood estimates to derive the true posterior probability distribution of the [B2017](#) and [S2017](#) parameters. Our parameter constraints reveal the impact of likelihood non-Gaussianity on the posterior parameter constraints of [B2017](#) and [S2017](#). Despite some impact on the $f\sigma_8$ constraint, likelihood non-Gaussianity does not significantly impact the overall [B2017](#) parameter constraints. For the ζ analysis, however, using the pseudo-likelihood significantly underestimates the uncertainties and biases the constraints of [S2017](#) halo occupation parameters: $\log M_{\min}$, $\log M_1$ and α . The divergence and likelihood estimation methods we present provides a straightforward framework for quantifying the impact of likelihood non-Gaussianity and deriving more accurate parameter constraints.

Subject headings: methods: statistical — galaxies: statistics — methods: data analysis — cosmology: observations — cosmological parameters — large-scale structure of universe

1. Introduction

Bayesian parameter inference has become the standard framework for deriving cosmological parameters of interest from observed measurements such as the galaxy powerspectrum or

two-point correlation function in large scale structure (LSS) studies and cosmology analyses in general. From Bayes rule,

$$p(\theta | x) \propto p(x | \theta)p(\theta). \quad (1)$$

the posterior parameter constraints can be calculated from the prior and the likelihood – probability of the data given the theoretical model. Since analyses choose priors, parameter inference ultimately boils down to evaluating the likelihood. Hence it goes without say that our analyses can only lead to unbiased constraints if the employed likelihood is correct.

In present day LSS analyses, two major assumptions go into evaluating the likelihood. First, the likelihood is assumed to have a Gaussian functional form. LSS analyses employ a Gaussian *pseudo*-likelihood. **sentence about how this is different than non-Gaussian terms in the covariance matrix.** Second, the covariance matrix used in evaluating the Gaussian pseudo-likelihood is assumed to be independent of the parameters θ . **explain in more detail.** The dependence of the covariance matrix on cosmological parameters has been shown to have a significant effect on parameter constraints (*e.g.* Eifler et al. 2009). In this paper, we focus on evaluating the impact of the first assumption (*i.e.* the Gaussian pseudo-likelihood) on cosmological parameter constraints.

The motivation for the Gaussian pseudo-likelihood ultimately stems from the Central Limit Theorem. The powerspectrum of the density field, for instance, is the correlation function of the density field. Assuming that the density field is a Gaussian random field, which it approximately is, the powerspectrum of a specific mode would follow a chi-squared distribution. With sufficiently many independent modes contributing, from Central Limit Theorem, the likelihood of the powerspectrum would *approach* a Gaussian distribution. In practice, due to finite survey volume, shot noise, and systematic effects different modes are correlated and the Gaussian likelihood assumption cannot be true for the powerspectrum. In low signal-to-noise regimes we explicitly expect the Gaussian assumption to fail. Scoccimarro (2000) **provides an excellent example of how the Gaussianity illustrates how the** this for the powerspectrum.

talk about CMB likelihood analyses? Bring up sellentin et al.’s t-distribution stuff? Hence for precise parameter constraints, LSS analyses using the Gaussian pseudo-likelihood must insure that their analysis is conducted in sufficiently high signal-to-noise regimes and test the impact of likelihood non-Gaussianity. This is unfortunately not a part of the standard practice in LSS studies.

In this paper we investigate the impact of the likelihood Gaussianity assumption on the two recent LSS analyses of Beutler et al. (2017) (hereafter B2017) and Sinha et al. (2017) (hereafter S2017). B2017 analyzes the powerspectrum multipoles (P_ℓ ; monopole, quadrupole, and hexadecapole) to measure redshift-space distortions along with the AlcockPaczynski effect and baryon acoustic oscillation scale. Meanwhile S2017 analyzes the group multiplicity function (ζ) in order constrain parameters of the halo model. Using

the [B2017](#) and [S2017](#) analyses, we show in this paper that the assumption of likelihood Gaussianity in LSS is not necessary. We will also show that the mock catalogs used in standard LSS analyses for covariance matrix estimation can be used to quantify the non-Gaussianity. More importantly the mocks can be used to estimate the “true” non-Gaussian likelihood.

We begin in [Section 2](#) by describing the mock catalogs, which we use throughout the paper, constructed originally for covariance matrix estimation in [B2017](#) and [S2017](#). Next in [Section 3](#), we present non-parametric divergence estimators and quantify the non-Gaussianity of the P_ℓ and ζ likelihoods using them. Then in [Section 4](#), we introduce two methods for estimating the “true” likelihood using the mock catalogs. We then use the likelihood estimates to quantify the impact of likelihood non-Gaussianity on the posterior parameter constraints of [B2017](#) and [S2017](#). We discuss and conclude the paper in [Section 6](#).

2. Mock Catalogs

Mock catalogs play an indispensable role in standard cosmological analyses of LSS studies. They’re used for testing analysis pipelines ([Beutler et al. 2017](#); [Grieb et al. 2017](#); [Tinker & et al. in preparation](#)), testing the effect of systematics ([Guo et al. 2012](#); [Vargas-Magaña et al. 2014](#); [Hahn et al. 2017a](#); [Pinol et al. 2017](#); [Ross et al. 2017](#)), and, most relevantly for this paper, estimating the covariance matrix ([Parkinson et al. 2012](#); [Kazin et al. 2014](#); [Grieb et al. 2017](#); [Alam et al. 2017](#); [Beutler et al. 2017](#); [Sinha et al. 2017](#)). In fact, nearly all current state-of-the-art LSS analyses use covariance matrices estimated from mocks to evaluate the likelihood for parameter inference.

While some argue for analytic estimates of the covariance matrix (e.g. [Mohammed et al. 2017](#)) or estimates directly from data by subsampling (e.g. [Norberg et al. 2009](#)), covariance matrices from mocks have a number of advantages. Mocks allow us to incorporate detailed systematic errors present in the data and variance beyond the volume of the data. Even for analytic estimates, a large ensemble of mocks are crucial for validation (e.g. [Slepian et al. 2017](#)). Moreover, as we show later in this paper, mocks present an additional advantage: they allow us to quantify the non-Gaussianity of the likelihood and more accurately estimate the true likelihood distribution.

In this paper, we focus on two LSS analyses: the powerspectrum multipole (P_ℓ) analysis of [B2017](#) and group multiplicity function (ζ) analysis of [S2017](#). Throughout the paper we will make extensive use of the mock catalogs used in these analyses. In this section, we give a brief description of these mocks and how the observables used in the analysis — the powerspectrum multipole (P_ℓ) and group multiplicity function (ζ) — are calculated from them. Afterwards, we will describe how we compute the covariance matrix from the mocks and pre-process the mock observable data.

2.1. MultiDark-PATCHY Mock Catalog

In their powerspectrum multipole analysis, B2017 use the MultiDark-PATCHY mock catalogs from Kitaura et al. (2016). These mocks are generated using the PATCHY code (Kitaura et al. 2014, 2015). They rely on large-scale density fields generated using augmented Lagrangian Perturbation Theory (ALPT; Kitaura & Heß 2013) on a mesh, which they then populate with galaxies based on a combined non-linear deterministic and stochastic biases. The mocks from the PATCHY code are then calibrated to reproduce the galaxy clustering in the high-fidelity BigMultiDark N -body simulation (Rodríguez-Torres et al. 2016; Klypin et al. 2016). Afterwards, the galaxies are assigned stellar masses using the HADRON code (Zhao et al. 2015). and the SUGAR code (Rodríguez-Torres et al. 2016) is applied to combine different boxes, incorporate selection effects and masking to produce mock light-cone galaxy catalogs. The statistics of the resulting mocks are then compared to observations and the process is iterated to reach desired accuracy. We refer readers to Kitaura et al. (2016) for further details.

In total, Kitaura et al. (2016) generated 12,228 mock light-cone galaxy catalogs for BOSS Data Release 12. In B2017, they use 2045 and 2048 for the northern galactic cap (NGC) and southern galactic cap (SGC) of the LOWZ+CMASS combined sample. B2017 excluded 3 mock realizations due to notable issues. These issues have since been addressed so in our analysis we use all 2048 mocks for both the NGC and SGC of the LOWZ+CMASS combined sample. In B2017, they conduct multiple analyses, some using only the powerspectrum monopole and quadrupole and others using monopole, quadrupole, and hexadecapole. They also separately analyze three redshift bins: $0.2 < z < 0.5$, $0.4 < z < 0.6$, and $0.5 < z < 0.75$. In this paper we focus on one of these analyses: the analysis of the powerspectrum monopole, quadrupole, and hexadecapole for the $0.2 < z < 0.5$ bin.

2.2. Sinha et al. (2017) Mocks

The simulations used in the small-scale clustering analysis of Sinha et al. (2017) are from the Large Suite of Dark Matter Simulations project (LasDamas; McBride et al. 2009) designed to model galaxy samples from SDSS DR7. They use initial conditions derived from second order Lagrangian Perturbation Theory using the 2LTPIC code (Scoccimarro 1998; Crocce et al. 2006) and evolved them using the N -body GADGET-2 code (Springel 2005). Halos are then identified from the dark matter distribution outputs using the `ntropy – fofsv` code (Gardner et al. 2007), which uses a friend-of-friends algorithm (FoF; Davis et al. 1985) with a linking length of 0.2 times the mean inter-particle separation. S2017 uses two configurations of the LasDamas simulations for the $M_r < -19$ and $M_r < -21$ samples of SDSS DR7. The Consuelo simulation contains 1400^3 dark matter particles with mass of $1.87 \times 10^9 h^{-1} M_\odot$ in a cubic volume of $420 h^{-1} Mpc$ per side evolved from $z_{\text{init}} = 99$. The Carmen simulation

contains 1120^3 dark matter particles with mass of $4.938 \times 10^{10} h^{-1} M_\odot$ in a cubic volume of $1000 h^{-1} \text{Mpc}$ per side evolved from $z_{\text{init}} = 49$.

The FoF halo catalogs are then populated with galaxies using the ‘Halo Occupation Distribution’ (HOD) framework. The number, positions, and velocities of galaxies are described statistically by an HOD model. S2017 adopts the ‘vanilla’ HOD model of Zheng et al. (2007), where the mean number of central and satellite galaxies are described by the halo mass and five HOD parameters: $M_{\text{min}}, \sigma_{\log M}, M_0, M_1$, and α . Lastly, once the simulation boxes are populated with galaxies, observational systematic effects are imposed. The peculiar velocities of galaxies are used to impose redshift-space distortions. Galaxies that lie outside the redshift limits or sky footprint of the SDSS sample are removed. For further details regarding the mocks, we refer readers to S2017.

To calculate their covariance matrix, S2017 produced 200 independent mock catalogs from 50 simulations using a single set of HOD model parameters. To take advantage of the methods we later present, we require a large number of mocks. Our methods rely on using the mocks to sample high dimensional distributions, so incorporating more mocks improves their accuracy. We utilize an addition 99 sets of HOD parameters with 200 mocks each. These parameters are sampled from the MCMC chain used to produce the posterior in S2017. In total we use 20,000 mocks. Among the multiple analyses in S2017, in this paper we focus on the GMF analysis of the SDSS DR7 $M_r < -19$ sample.

2.3. Mock Observable \mathbf{X}^{mock} and Covariance Matrix \mathbb{C}

To get from the mock catalogs described above to the covariance matrices used in B2017 and S2017, the observables are measured for each mock in the *same* way as the observations. We briefly describe how $P_\ell(k)$ and $\zeta(N)$ and their covariance matrices are measured in B2017 and S2017. We then describe how we pre-process the mock observables for the methods we describe in the next sections.

To measure the powerspectrum multipoles of the BOSS DR12 galaxies and the MutliDark-PATCHY mocks (Section 2.1), B2017 uses a fast Fourier transform (FFT) based anisotropic powerspectrum estimator based on Bianchi et al. (2015) and Scoccimarro (2015). This estimator estimates the monopole, quadrupole, and hexadecapole ($\ell = 0, 2$, and 4) of the powerspectrum using FFTs of the overdensity field multipoles for a given survey geometry. For further details on the estimator we refer readers to B2017 Section 3. B2017 compute the powerspectrum over the range $k = 0.01 - 0.15 h \text{Mpc}^{-1}$ for $\ell = 0$, and 2 and $k = 0.01 - 0.10 h \text{Mpc}^{-1}$ for $\ell = 4$. The powerspectrum multipoles are calculated in bins of $\Delta k = 0.01 h \text{Mpc}^{-1}$.

From the $\vec{P}^{(n)} = [P_0^{(n)}(k), P_2^{(n)}(k), P_4^{(n)}(k)]$ of the MultiDark-PATCHY mocks, B2017 com-

putes the (i, j) element of the covariance matrix of all multipoles as

$$\mathbb{C}_{i,j} = \frac{1}{N_{\text{mock}} - 1} \sum_{n=1}^{N_{\text{mock}}} [\vec{P}_i^{(n)} - \bar{P}_i] \times [\vec{P}_j^{(n)} - \bar{P}_j]. \quad (2)$$

$N_{\text{mock}} = 2048$ is the number of mocks and \bar{P}_i is the mean of the mock powerspectra: $\bar{P}_i = \frac{1}{N_{\text{mock}}} \sum_{n=1}^{N_{\text{mock}}} \vec{P}_i^{(n)}$. Since P_0 and P_2 each have 14 bins and P_4 has 9 bins, \mathbb{C} is a 37×37 matrix. In this work, we compute the $P_\ell(k)$ using a similar FFT-based estimator of [Hand et al. \(2017b\)](#) instead of the [B2017](#) estimator. Our choice is based on computational convenience. A python implementation of the [Hand et al. \(2017b\)](#) estimator is publicly available in the NBODYKIT package³ ([Hand et al. 2017a](#)). We confirm that the resulting $P_\ell(k)$ s and covariance matrices from the two estimators are consistent with one another.

Next, for the [S2017](#) group multiplicity function analysis, they start with the [Berlind et al. \(2006\)](#) FoF algorithm to identify groups in the SDSS and mock data. [S2017](#) adopts the [Berlind et al. \(2006\)](#) linking lengths in units of mean inter-galaxy separation: $b_\perp = 0.14$ and $b_\parallel = 0.75$. In comoving lengths, the linking lengths for the SDSS DR7 $M_r < -19$ sample correspond to $(r_\perp, r_\parallel) = (0.57, 3.05)h^{-1}$ Mpc. Once the groups are identified in the SDSS and mock data, $\zeta(N)$ is derived by calculating the comoving number density of groups in bins of richness N — the number of galaxies in the group. For the $M_r < 19$ SDSS sample, [S2017](#) uses eight N bins: $(5 - 6)$, $(7 - 9)$, $(10 - 13)$, $(14 - 19)$, $(20 - 32)$, $(33 - 52)$, $(53 - 84)$, $(85 - 220)$. For further details on the GMF calculation, we refer readers to [S2017](#) Section 4.2. From the $\zeta^{(n)}(N)$ s of each mock, [S2017](#) computes the (i, j) element of the covariance matrix as

$$\mathbb{C}_{i,j} = \frac{1}{N_{\text{mock}} - 1} \sum_{n=1}^{N_{\text{mock}}} [\zeta^{(n)}(N_i) - \bar{\zeta}(N_i)] \times [\zeta^{(n)}(N_j) - \bar{\zeta}(N_j)]. \quad (3)$$

In [S2017](#), they compute the covariance matrix using 200 mocks generated using a single fiducial set of HOD parameters. As we describe in Section 2.2, in this paper we use 20,000 mocks from 100 different set of HOD parameters sampled from the MCMC chain. The GMF covariance matrix we use in this paper is computed with $N_{\text{mock}} = 20,000$ mocks.

For the rest of the paper, in order to discuss the two separate analyses of [B2017](#) and [S2017](#) in a consistent manner, we define the matrix \mathbf{D}^{mock} of the mock observables (P_ℓ and ζ) as

$$\mathbf{D}^{\text{mock}} = \left\{ \mathbf{D}_n^{\text{mock}} \right\} \quad \text{where } \mathbf{D}_n^{\text{mock}} \begin{cases} \vec{P}^{(n)} & \text{for B2017,} \\ \zeta^{(n)} & \text{for S2017.} \end{cases} \quad (4)$$

\mathbf{D}^{mock} has dimensions of 2048×37 and $20,000 \times 8$ for [B2017](#) and [S2017](#) respectively.

³<http://nbodykit.readthedocs.io/en/latest/index.html>

For the methods in Sections 4.1 and 4.2, the mock observable data (\mathbf{D}^{mock}) need to be pre-processed. This pre-processing involves two steps: mean-subtraction (centering) and whitening. For mean subtraction, the mean of the observable is subtracted from \mathbf{D}^{mock} . Then $\mathbf{D}^{\text{mock}} - \bar{\mathbf{D}}^{\text{mock}}$ is whitened using a linear transformation to remove the Gaussian correlation between the bins of \mathbf{D}^{mock} :

$$\mathbf{X}^{\text{mock}} = L (\mathbf{D}^{\text{mock}} - \bar{\mathbf{D}}^{\text{mock}}). \quad (5)$$

The linear transformation is derived so that covariance matrix of the whitened data, \mathbf{X}^{mock} , is the identity matrix \mathbb{I} . Such a whitening linear transformation can be derived in infinite ways. One way to derive the linear transformation is through the eigen-decomposition of the covariance matrix (*e.g.* Hartlap et al. 2009; Sellentin et al. 2017). We, alternatively, derive the linear transformation \mathbf{L} using Cholesky decomposition of the inverse covariance matrix (Press et al. 1992): $\mathbb{C}^{-1} = \mathbf{L}\mathbf{L}^T$. The different methods for whitening do not impact the results of the paper. Now that we have the pre-processed data of the mock observables, we proceed in the next section to quantifying the non-Gaussianity of the P_ℓ and ζ likelihoods.

3. Quantifying the Likelihood non-Gaussianity

The standard approach to parameter inference in LSS studies neglects to account for likelihood non-Gaussianity. However, we are not the first to investigate likelihood non-Gaussianity in LSS analyses. Nearly two decades ago, Scoccimarro (2000) examined the likelihood non-Gaussianity for the powerspectrum and reduced bispectrum using mock catalogs of the IRAS redshift catalogs. More recently, Hartlap et al. (2009) and Sellentin et al. (2017) examined the non-Gaussianity of the cosmic shear correlation function likelihood using simulations of the Chandra Deep Field South and CFHTLenS, respectively.

While these works present different methods for identifying likelihood non-Gaussianity, they do not present a concrete way of quantifying it. Hartlap et al. (2009), for instance, identifies the non-Gaussianity of the cosmic shear likelihood by looking at the statistical independence/dependence of PCA components of the mock observable. In Sellentin et al. (2017), they use the Mean Integrated Squared Error (MISE) as a distance metric between Gaussian random variables and the whitened mock observable data vector to characterize non-Gaussian correlations between elements of the data vector. These indirect measures of non-Gaussianity are challenging to interpret and extend more generally to LSS studies.

A more direct approach, however, can be taken to quantify the non-Gaussianity of the likelihood. We can calculate the divergence between the distribution of our observable, $p(x)$, and $q(x)$ a multivariate Gaussian described by the average of the mocks and the covariance matrix. The following are two of the most commonly used divergences: the Kullback-Leibler

(KL) divergence

$$D_{KL}(p \parallel q) = \int p(x) \log \frac{p(x)}{q(x)} dx \quad (6)$$

and the Rényi- α divergence

$$D_{R-\alpha}(p \parallel q) = \frac{1}{\alpha - 1} \log \int p^\alpha(x) q^{1-\alpha}(x) dx. \quad (7)$$

In the limit as α approaches 1, the Rényi- α divergence is equivalent to the KL divergence.

Of course, in our case, we don't know $p(x)$ — *i.e.* the distribution of our observable. If we did, we would simply use that instead of bothering with the covariance matrix or this paper. We can, however, still estimate the divergence using nonparametric divergence estimators (Wang et al. 2009; Póczos et al. 2012; Krishnamurthy et al. 2014). These estimators allow us to estimate the divergence directly from samples $X_{1:n} = \{X_1, \dots, X_n\}$ and $Y_{1:m} = \{Y_1, \dots, Y_m\}$ drawn from p and q respectively: $\hat{D}_\alpha(X_{1:n} \parallel Y_{1:m})$. For instance, the estimator presented in Póczos et al. (2012) allows us to estimate the kernel function of the Rényi- α divergence,

$$D_\alpha(p \parallel q) = \int p^\alpha(x) q^{1-\alpha}(x) dx. \quad (8)$$

using k^{th} nearest neighbor density estimators. Let $\rho_k(x)$ denote the Euclidean distance of the k^{th} nearest neighbor of x in the sample $X_{1:n}$ and $\nu_k(x)$ denote the Euclidean distance of the k^{th} nearest neighbor of x in the sample $Y_{1:m}$. Then

$$D_\alpha(p \parallel q) \approx \hat{D}_\alpha(X_{1:n} \parallel Y_{1:m}) = \frac{B_{k,\alpha}}{n} \left(\frac{n-1}{m} \right)^{1-\alpha} \sum_{i=1}^n \left(\frac{\rho_k^d(X_i)}{\nu_k^d(X_i)} \right)^{1-\alpha}, \quad (9)$$

where $B_{k,\alpha} = \frac{\Gamma(k)^2}{\Gamma(k-\alpha+1)\Gamma(k+\alpha-1)}$. This estimator, as Póczos et al. (2012) proves, is asymptotically unbiased,

$$\lim_{n,m \rightarrow \infty} \mathbb{E}[\hat{D}_\alpha(X_{1:n} \parallel Y_{1:m})] = D_\alpha(p \parallel q). \quad (10)$$

Plugging $\hat{D}_\alpha(X_{1:n} \parallel Y_{1:m})$ into Eq. 7, we get an estimator for the Rényi- α divergence. Wang et al. (2009) derives a similar estimator for the KL divergence (Eq. 6). These divergence estimates have been applied to Support Distribution Machines and used in the machine learning and astronomical literature with great success (*e.g.* Póczos et al. 2011, 2012; Póczos et al. 2012a,b; Xu et al. 2013; Ntampaka et al. 2015, 2016; Ravanbakhsh et al. 2017). For more details on the non-parametric divergence estimators, we refer readers to Póczos et al. (2012) and Krishnamurthy et al. (2014).

With these estimators, we can now explicitly quantify the non-Gaussianity of the likelihood by computing the divergence between the likelihood distribution and the Gaussian pseudo-likelihood distribution, $\mathcal{L}^{\text{pseudo}}$: $D(p(x) \parallel \mathcal{L}^{\text{pseudo}})$. We draw a reference sample \mathbf{Y}^{ref}

from $\mathcal{L}^{\text{pseudo}}$ then since \mathbf{X}^{mock} is in principle sampled from $p(x)$, we can use the estimators to compute $\hat{D}(\mathbf{X}^{\text{mock}} \parallel \mathcal{L}^{\text{pseudo}})$. Similar to the experiments detailed in Póczos et al. (2012), we construct \mathbf{Y}^{ref} with a comparable sample size as \mathbf{X}^{mock} : 2000 and 10,000 for the P_ℓ and ζ analyses respectively. Furthermore, based on the sample size of \mathbf{X}^{mock} we calculate the divergences using the $k = 10$ nearest neighbors.

In Figure 1, we present the resulting Rényi- α (left) and KL (right) divergences (orange) between the likelihood and the Gaussian pseudo-likelihood for the B2017 P_ℓ (top) and S2017 ζ (bottom) analyses: $\hat{D}_{R\alpha}$ and \hat{D}_{KL} . For reference, we also include (in blue) divergence estimates of the pseudo-likelihood onto itself, which we calculate as $\hat{D}(\mathbf{X}^{\text{ref}} \parallel \mathbf{Y}^{\text{ref}})$. \mathbf{X}^{ref} is a data vector with the same dimension as \mathbf{X}^{mock} sampled from the pseudo-likelihood \mathcal{N} . \hat{D} s are *estimates* of the true divergence, therefore we resample \mathbf{Y}^{ref} and compute each \hat{D} 100 times. Figure 1 actually presents the \hat{D} distributions, which also illustrate the uncertainty of \hat{D} . The discrepancy between the $\hat{D}(p(x) \parallel \mathcal{L}^{\text{pseudo}})$ distributions and the reference $\hat{D}(\mathbf{X}^{\text{ref}} \parallel \mathbf{Y}^{\text{ref}})$ distributions ($\Delta\hat{D}$) quantify the discrepancy between the pseudo-likelihood and the likelihood. Each panel of Figure 1 shows significant discrepancy between the two distributions — *both the $P_\ell(k)$ and $\zeta(N)$ likelihoods are significantly non-Gaussian*.

The Gaussian pseudo-likelihood assumption for P_ℓ is motivated by the Central Limit Theorem. If enough modes contribute to the powerspectrum, then the likelihood approaches a Gaussian. Given the survey volume of BOSS DR12 and the restrictive k range of the B2017 analysis ($0.01 < k < 0.15$ for $\ell = 0$ and 2; $0.01 < k < 0.15$ for $\ell = 4$), one would expect this to be mostly true. Although relatively small, we still find significant $\Delta\hat{D}$ and therefore likelihood non-Gaussianity. In order to better understand the source of this non-Gaussianity, we repeat the divergence comparisons for different k ranges. If we set $k_{\text{min}} = 0.05$, $\Delta\hat{D}$ decreases. Meanwhile, when we set $k_{\text{max}} = 0.1$ for all multipoles, $\Delta\hat{D}$ increases. This suggests that the P_ℓ likelihood is most non-Gaussian on large scales (low k). Furthermore, when we compare the divergences for just the monopole and quadrupole, $\Delta\hat{D}$ decreases. Among the multipole, the hexadecapole contributes most to the non-Gaussianity of the P_ℓ likelihood.

For ζ , the discrepancies between the \hat{D} distributions are consistent with the fact that the true ζ likelihood distribution is likely Poisson — not Gaussian — similar to the likelihood of observed cluster counts (Cash 1979; Collaboration et al. 2014; Ade et al. 2016). Although the groups identified with a FoF algorithm do not correspond to clusters, we nevertheless expect the likelihood to be non-Gaussian. We again repeat the divergence comparison for different N ranges to better understand the source of non-Gaussianity. Excluding the lowest N bin does not significantly impact $\Delta\hat{D}$. However, when we exclude the highest N bin, $\Delta\hat{D}$ decreases significantly. We therefore find that the high richness end of ζ contribute most to the non-Gaussianity of the ζ likelihood.

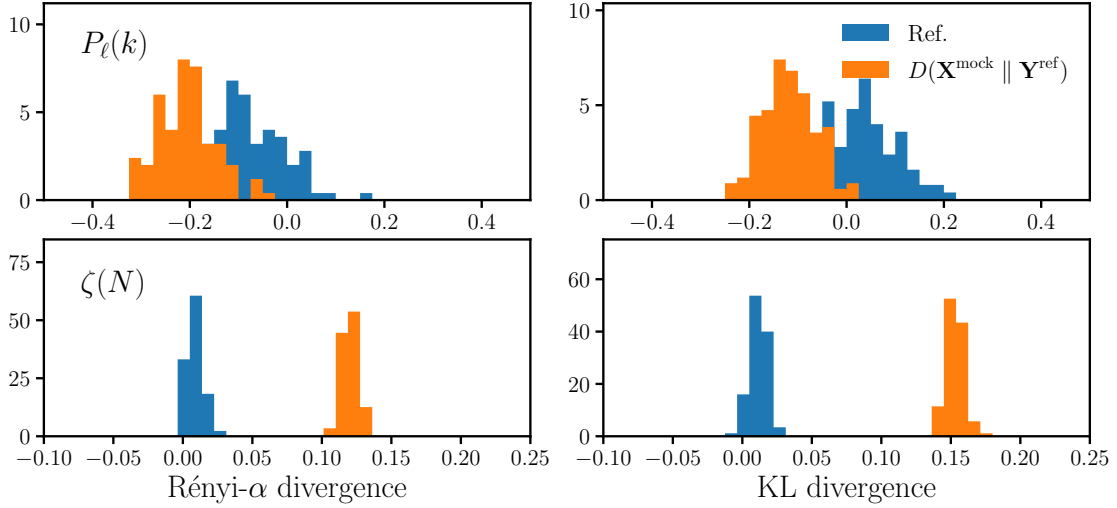


Fig. 1.— Rényi- α and KL divergence estimates ($\hat{D}_{R\alpha}$ and \hat{D}_{KL} ; orange) between the likelihood distribution and the Gaussian pseudo-likelihood for the [B2017](#) P_ℓ (top) and [S2017](#) ζ (bottom) analyses. We include in blue, as reference, the divergence estimates of the pseudo-likelihood onto itself. $\hat{D}_{R\alpha}$ and \hat{D}_{KL} are computed using the non-parametric k -NN estimator (Section 3) on the mock data \mathbf{X}^{mock} and a reference sample \mathbf{Y}^{ref} drawn from the pseudo-likelihood. We compute $\hat{D}_{R\alpha}$ and \hat{D}_{KL} **100** times and plot their distribution in order to illustrate the uncertainty in the \hat{D} estimator. The significant discrepancy between the two divergence distributions in each of the panels, identifies the *significant non-Gaussianity of the $P_\ell(k)$ and $\zeta(N)$ likelihoods*.

4. Estimating the Non-Gaussian Likelihood

In the previous section, we estimate the divergence between the P_ℓ and ζ likelihoods sampled by mocks and their respective Gaussian pseudo-likelihoods. These divergences identify and quantify the significant non-Gaussianity in the likelihoods of LSS studies. Our ultimate goal, however, is to quantify the impact of likelihood non-Gaussianity on the final cosmological parameter constraints and to develop more accurate methods for parameter inference in LSS. From the divergence estimates alone, it’s not obvious how they propagate onto the final parameter constraints. Therefore in this section, we present two methods for more accurately estimating the non-Gaussian likelihoods of P_ℓ and ζ from the corresponding mocks. These methods provide a more accurate estimate of the likelihood than the Gaussian pseudo-likelihood. Moreover, we will use them later to quantify the impact of likelihood non-Gaussianity on the [B2017](#) and [S2017](#) parameter constraints.

4.1. Gaussian Mixture Likelihood Estimation

When mock catalogs are used for parameter inference in LSS analyses, they essentially serve as data points sampling the likelihood distribution. For the pseudo-likelihood, this distribution is assumed to have a Gaussian functional form. Hence, why we estimate the covariance matrix from mocks. However, the Gaussian functional form, or any functional form for that matter, is *not* necessary to estimate the likelihood distribution. Instead, the multidimensional likelihood distribution can be directly estimated from the set of mock catalogs using — for instance using Gaussian mixture density estimation ([Press et al. 1992](#); [McLachlan & Peel 2000](#)). Besides its extensive use in machine learning and statistics, in astronomy, Gaussian mixture density estimation has been used for inferring the velocity distribution of stars from the Hipparcos satellite ([Bovy et al. 2011](#)), classifying galaxies in the Galaxy And Mass Assembly Survey ([Taylor et al. 2015](#)), and classifying pulsars ([Lee et al. 2012](#); see also [Hogg et al. 2010](#); [Kuhn & Feigelson 2017](#)).

Gaussian mixture density estimation is a “semi-parametric” method that uses a weighted sum of k Gaussian component densities, a Gaussian mixture model (hereafter GMM)

$$p(x; \boldsymbol{\theta}) = \sum_{i=1}^k \pi_i \mathcal{N}(x; \boldsymbol{\theta}_i), \quad (11)$$

to estimate the density. The component weights (π_i ; also known as mixing weights) and the component parameters $\boldsymbol{\theta}_i$ are free parameters of the mixture model. Given some data set $\mathbf{X}_N = \{\mathbf{x}_1, \dots, \mathbf{x}_N\}$, these free GMM parameters are, most popularly, estimated through an expectation-maximization algorithm (EM; [Dempster et al. 1977](#); [Neal & Hinton 1998](#)). The EM algorithm begins by randomly assigning $\boldsymbol{\theta}_i^0$ to the k Gaussian components. The algorithm then iterates between two steps. In the first step, the algorithm computes for each

data point, \mathbf{x}_n , a probability of being generated by each component of the model. These probabilities can be thought of as weighted assignments of the points to the components. Next, given the \mathbf{x}_n assignment to the components, $\boldsymbol{\theta}_i^t$ of each component are updated to $\boldsymbol{\theta}_i^{t+1}$ to maximize the likelihood of the assigned points. At this point, π_i can also be updated by summing up the assignment weights and normalizing it by the total number of data points, N . This entire process is repeated until convergence — *i.e.* when the log-likelihood of given the mixture model $\log p(\mathbf{X}_N; \boldsymbol{\theta}^t)$ converges. The EM algorithm is guaranteed to converge to a local maximum of the likelihood (Wu 1983).

In practice, instead of arbitrarily assigning the initial condition, $\boldsymbol{\theta}_i^0$ is derived from a **k-means** clustering algorithm (Lloyd 1982). Without going into details, the **k-means** algorithm clusters the data \mathbf{X}_N into k clusters, each described by the mean (or centroid) μ_i of the samples in the cluster. The algorithm then iteratively chooses centroids that minimize the average squared distance between points in the same cluster. For our GMMs, we set the initialize the EM algorithm using the **k-means++** algorithm of Arthur & Vassilvitskii (2007). In Figure 2, we illustrate Gaussian mixture density estimation in action. We use GMMs with $k = 1$ (top), 3 (middle), and 10 (bottom) components to estimate the distribution of one dimensional data (blue) drawn from three separate Gaussian distributions. The GMM outputs of the EM algorithm are plotted in red with dotted black lines representing each of their components.

So far in our description of GMMs, we have kept the number of components k fixed. However, k is a free parameter and selecting it is a crucial step in Gaussian mixture density estimation. With too many components the model may overfit the data; with too few components, the model may not be flexible enough to approximate the true underlying distribution. In order to address this model selection problem of selecting k , we make use of the Bayesian Information Criterion (BIC; Schwarz 1978). BIC has been widely used for determining the number of components in mixture modeling (*e.g.* Leroux 1992; Roeder & Wasserman 1997; Fraley & Raftery 1998; Steele & Raftery 2010) and for model selection in general in astronomy (*e.g.* Liddle 2007; Broderick et al. 2011; Wilkinson et al. 2015; Vakili & Hahn 2016). According to BIC, models with higher likelihood are preferred; however, to address the concern of overfitting, BIC introduces a *penalty* term for the number of parameters in the model:

$$\text{BIC} = -2 \ln \mathcal{L} + N_{\text{par}} \ln N_{\text{data}}. \quad (12)$$

We select k based on the number of components in the model with the lowest BIC. Of the three panels in Figure 2, the GMM model with $k = 3$ components has the lowest BIC and therefore would be selected. At least in this example, the choice of $k = 3$ is obviously justified. The $k = 1$ GMM is definitely not flexible enough to characterize the underlying distribution and the $k = 10$ GMM clearly overfits the distribution.

With Gaussian mixture density estimation we can directly estimate the likelihood dis-

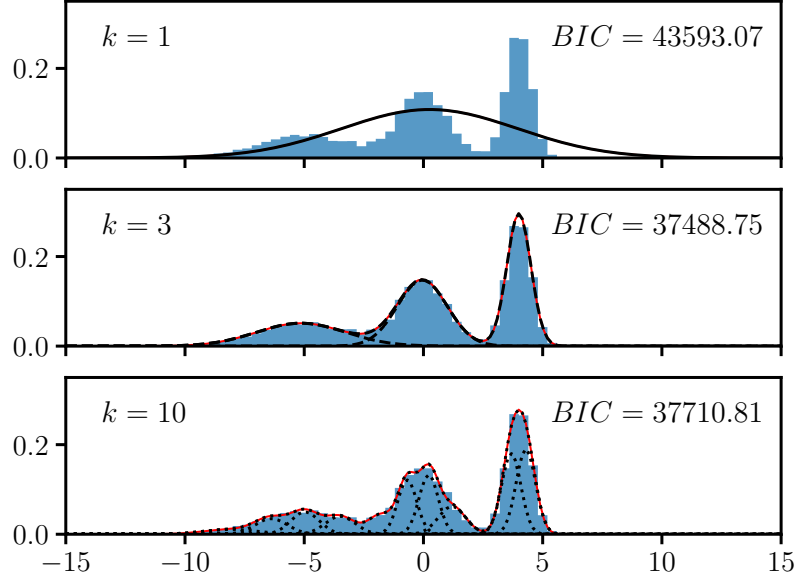


Fig. 2.— A pedagogical illustration of Gaussian mixture density estimation. We use GMMs with $k = 1$ (top), 3 (middle), 10 (bottom) components to estimate the distribution of data (blue) drawn from three Gaussian distributions. The GMM outputs of the EM algorithm are plotted in red with **dotted lines** representing each of their components (Section 4.1). We also include the BIC of the GMMs, which we use to select the number of components k . Of the three panels, $k = 3$ has the lowest BIC and therefore best represents the data according to our selection scheme.

tribution using the mock catalogs. We first fit GMMs with $ks < 30$ components to the whitened mock data \mathbf{X}^{mock} using the EM algorithm for each model. For each of the converged GMMs, we calculate the BIC. Afterwards we select the model with the lowest BIC as the best density estimate of the likelihood distribution: $\hat{p}_{\text{GMM}}(x)$. The selected density estimate can then be used to calculate the likelihood and quantify the impact of likelihood non-Gaussianity on the parameter constraints of B2017 and S2017. But before we do that, we have to confirm whether \hat{p}_{GMM} is in fact a better estimate of the likelihood over the Gaussian pseudo-likelihood. To do this, we return to the divergence estimates of Section 3.

To estimate the divergence between our Gaussian mixture density estimate, \hat{p}_{GMM} , and the likelihood distribution, we take the same approach as our \hat{D} calculation in Section 3. Instead of \mathbf{Y}^{ref} drawn from the pseudo-likelihood, we draw samples from $\hat{p}_{\text{GMM}}(x)$ with the same dimensions. Then we calculate k -NN Rényi- α and KL divergence estimates between this sample and \mathbf{X}^{mock} . As we did in Figure 1, we repeat this process 100 times, resampling \hat{p}_{GMM} each time, in order get a distribution of divergence estimates that reflects the scatter in the estimator. In Figure 3, we present the resulting distribution of divergences between \hat{p}_{GMM} and the likelihood distribution in green for the $P_\ell(k)$ (top) and $\zeta(N)$ (bottom) analyses. For comparison, we include the distributions from Figure 1.

For the $\zeta(N)$ analysis of S2017, our Gaussian mixture density estimate significantly improves the divergence discrepancy compared to the pseudo-likelihood. In other words, *our Gaussian mixture density estimate is a significant better estimate of the ζ likelihood distribution than the pseudo-likelihood*. On the other hand, our Gaussian mixture density estimate for the $P_\ell(k)$ analysis of B2017 does not significantly improve the divergence discrepancy. This difference in the performance of Gaussian mixture density estimation is not surprising. One would expect a direct density estimation to be more effective for the S2017 case, where we estimate an 8-dimensional distribution with $N_{\text{mock}} = 20,000$ samples, compared to the B2017 case where we estimate a 37-dimensional distribution with only $N_{\text{mock}} = 2048$ samples. Given the unconvincing accuracy of the Gaussian mixture density estimate of the P_ℓ likelihood, in the next section we present an alternative method for estimating the non-Gaussian likelihood.

4.2. Independent Component Analysis

Gaussian mixture density estimation fails to accurately estimate the 37-dimensional P_ℓ likelihood distribution of B2017. Rather than estimating the likelihood distribution directly, if we can transform the observable \mathbf{x} (e.g. P_ℓ) into statistically independent components \mathbf{x}^{IC} the problem becomes considerably simpler. Since \mathbf{x}^{IC} is statistically independent the

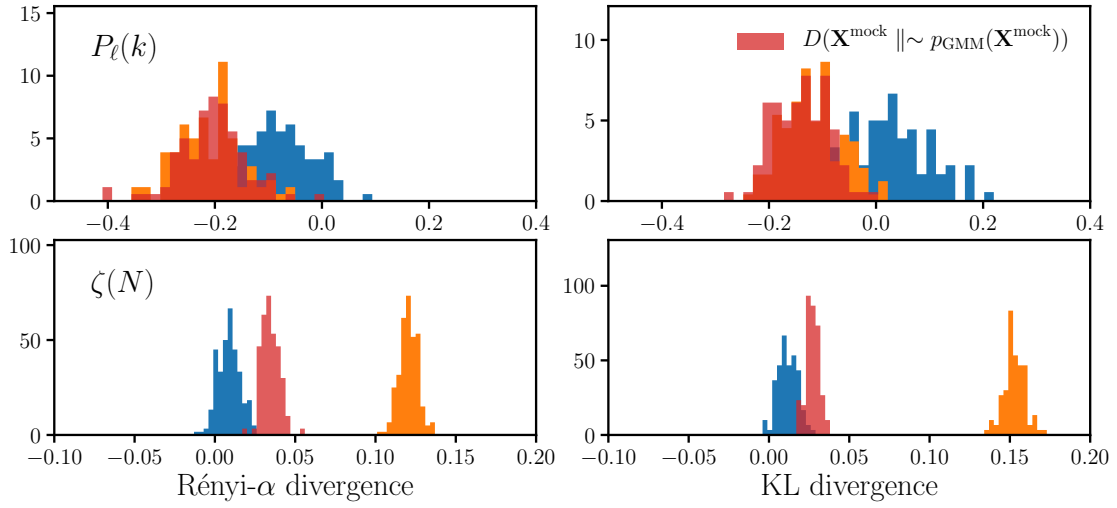


Fig. 3.— Rényi- α and KL divergence estimates ($\hat{D}_{R\alpha}$ and \hat{D}_{KL} ; **green**) between the likelihood distribution and the Section 4.1 GMM likelihood estimate for the [B2017](#) P_ℓ (top) and [S2017](#) ζ (bottom) analyses. We include the divergence estimates from Figure 1 for comparison. The Gaussian mixture likelihood does not significantly improve the discrepancy in divergence for the P_ℓ analysis. This is due to the high-dimensionality (37 dimensions) of the P_ℓ likelihood. However, for the ζ analysis, *our Gaussian mixture likelihood estimate is a significantly better estimate of the likelihood than the pseudo-likelihood*.

likelihood distribution becomes

$$p(x) = \prod_{n=1}^{N_{\text{bin}}} p_{x_n^{\text{IC}}}(x) \quad (13)$$

where N_{bin} is the number of bins in the observable. For the [B2017](#) case, this reduces the problem of estimating a 37 dimensional distribution with 2048 samples to a problem of estimating 37 one dimensional distributions with 2048 samples each. The challenge, however, is in finding the transformation.

Efforts in the past have attempted to tackle this sort of high-dimensional problem (*e.g.* [Scoccimarro 2000](#); [Eisenstein & Zaldarriaga 2001](#); [Gaztañaga & Scoccimarro 2005](#); [Norberg et al. 2009](#); [Sinha et al. 2017](#)). They typically use singular value decomposition or principal component analysis (PCA; [Press et al. 1992](#)). For a Gaussian likelihood, the PCA components of it are statistically independent. However, when the likelihood is *not* Gaussian, the PCA components are uncorrelated but *not necessarily statistically independent* ([Hartlap et al. 2009](#)). Since the P_ℓ and ζ likelihoods are non-Gaussian, we cannot use PCA. Instead, we follow [Hartlap et al. \(2009\)](#) and use Independent Component Analysis (ICA [Hérault & Ans 1984](#); [Comon 1994](#); [Hyvärinen & Oja 2000](#); [Hyvarinen 2001](#)).

In order to find the transformation of \mathbf{x} to \mathbf{x}^{IC} we first assume that \mathbf{x} is generated by some linear transformation $\mathbf{x} = \mathbf{M} \mathbf{x}^{\text{IC}}$. The goal of ICA is to invert this problem, $\mathbf{y} = \mathbf{W} \mathbf{x}$, and find \mathbf{W} and \mathbf{y} that best estimate $\mathbf{y} \approx \mathbf{x}^{\text{IC}}$. The basic premise of ICA is simple, *maximizing non-Gaussianity maximizes the statistical independence*. Consider a single component of \mathbf{y} :

$$\mathbf{y}_n = \mathbf{w}_n^t \mathbf{x} = \mathbf{w}_n^t \mathbf{M} \mathbf{x}^{\text{IC}} \quad (14)$$

where \mathbf{w}_n^t is the n^{th} row of \mathbf{W} . Since \mathbf{y}_n is a linear combination of the independent components \mathbf{x}^{IC} , due to the Central Limit Theorem \mathbf{y}_n is necessarily more Gaussian than any of the components *unless* \mathbf{y}_n is equal to one of the \mathbf{x}^{IC} components. In other words, we can achieve $\mathbf{y} \approx \mathbf{x}^{\text{IC}}$ by finding \mathbf{W} that maximizes the non-Gaussianity of \mathbf{y} . For a more rigorous justification of ICA we refer readers to [Hyvarinen \(2001\)](#). In practice, non-Gaussianity is commonly measured using differential entropy — “negentropy”. For \mathbf{y}_n with density function p_{y_n} the entropy is defined as

$$H_{y_n} = - \int p_{y_n}(y) \log p_{y_n}(y) dy. \quad (15)$$

Since the Gaussian distribution has the largest entropy among all distributions with a given variance, the negentropy can be defined as,

$$J_{y_n} = H_{y_n^{\text{Gauss}}} - H_{y_n}. \quad (16)$$

Finding the statistically independent components is now a matter of finding the \mathbf{W} that maximizes $\sum_n J_{y_n}$ — the negentropy of \mathbf{y} . In this paper, we make use of the **FastICA** fixed-point iteration algorithm ([Hyvarinen 1999](#)). The algorithm starts with randomly selected

$\mathbf{w}_n s$, then it uses approximations of negentropy from Hyvärinen (1998) and Newton’s method to iteratively solve for \mathbf{W} that maximizes negentropy. For details on the FastICA algorithm, we refer readers to Hyvärinen (1999).

Performing ICA on the whitened observable data \mathbf{X}^{mock} , we derive the matrix \mathbf{W} that transforms \mathbf{X}^{mock} into N_{bin} approximately independent components:

$$\mathbf{X}^{\text{ICA}} = \mathbf{W} \mathbf{X}^{\text{mock}} = \{\mathbf{X}_1^{\text{ICA}}, \dots, \mathbf{X}_{N_{\text{bin}}}^{\text{ICA}}\}. \quad (17)$$

From these statistically independent components and Eq. 13, we can estimate the likelihood distribution. $p_{x_n^{\text{IC}}}(x)$, from Eq. 13, is the 1-dimensional distribution function of the n^{th} ICA component. This distribution is sampled by $\mathbf{X}_n^{\text{ICA}}$, the transformed mock data. That means $\mathbf{X}_n^{\text{ICA}}$ can be used to estimate $p_{x_n^{\text{ICA}}}$ using a method like kernel density estimation (KDE; e.g. Hastie et al. 2009; Feigelson & Babu 2012). With KDE, the density estimate, $\hat{p}_{x_n^{\text{ICA}}}$, is constructed by smoothing the empirical distribution of the ICA component x_n^{ICA} using a smooth kernel:

$$\hat{p}_{x_n^{\text{ICA}}}(x) = \frac{1}{N_{\text{mock}} b} \sum_{j=1}^{N_{\text{mock}}} K \left(\frac{x - X_n^{(j), \text{ICA}}}{b} \right). \quad (18)$$

b is the bandwidth and K is the kernel function. Following the choices of Hartlap et al. (2009), we use a Gaussian distribution for K and the “rule of thumb” bandwidth (also known as Scott’s rule; Scott 1992; Davison 2008) for b . Combining $\hat{p}_{x_n^{\text{ICA}}}$ s estimates for all $n = 1, \dots, N_{\text{bin}}$ into Eq. 13, we can estimate the likelihood distribution $p(x) \approx \prod_n \hat{p}_{x_n^{\text{ICA}}}(x)$

We again test whether the likelihood estimate from ICA is actually a better estimate of the likelihood distribution than the Gaussian pseudo-likelihood. Following the same procedure as we did for the Gaussian mixture likelihood in Section 4.1, we calculate the divergence between our ICA likelihood, $\prod \hat{p}_{x_n^{\text{ICA}}}(x)$, and the likelihood distribution, $p(x)$. We draw a sample from $\prod \hat{p}_{x_n^{\text{ICA}}}$ with the same dimensions as \mathbf{Y}^{ref} (Section 3), apply the mixing matrix (undoing the ICA transformation), and then calculate the k -NN Rényi- α and KL divergence estimates between the sample and \mathbf{X}^{mock} . We repeat these steps 100 times to get the distribution of estimates that reflects the scatter in the estimator. In Figure 4, we present the resulting distribution of $\hat{D}(\mathbf{X}^{\text{mock}} \parallel \sim \prod \hat{p}_{x_n^{\text{ICA}}})$ in green for the $P_\ell(k)$ (top) and $\zeta(N)$ (bottom) analyses. For comparison, we include the distributions from Figure 1.

For both B2017 and S2017, our ICA likelihood significantly improves the divergence discrepancy compared to the pseudo-likelihood. For S2017, however, the ICA likelihood proves to be less accurate than the Gaussian mixture likelihood in Section 4.1. More importantly, for B2017, where the Gaussian mixture likelihood did not improve upon the pseudo-likelihood, the ICA method provides a significantly more accurate likelihood estimate. This demonstrates that the ICA method is an alternative to the more direct Gaussian mixture method. Furthermore, the effectiveness of the ICA method in estimating higher dimensional likelihoods with fewer samples (mocks) is particularly appealing for LSS, since analyses continue

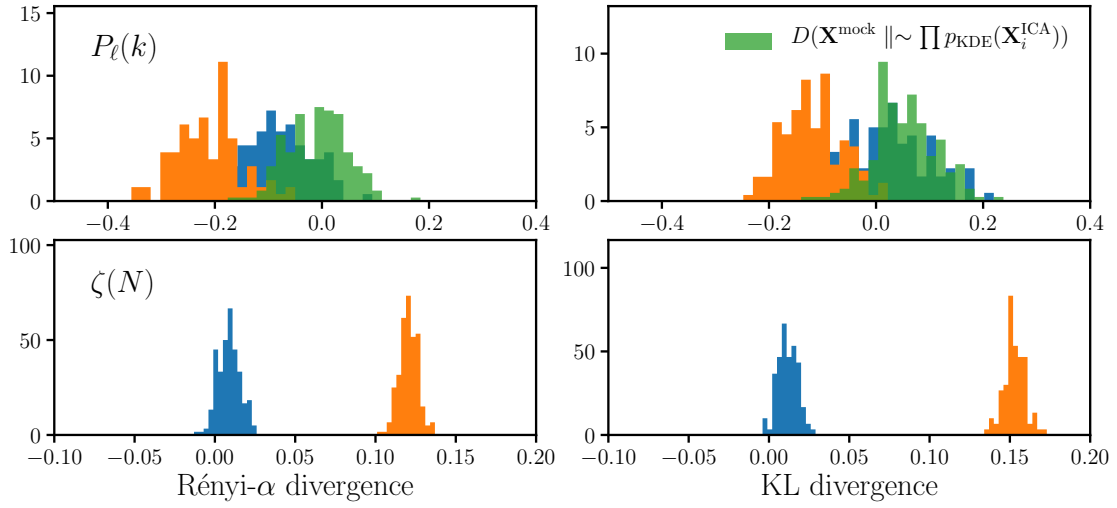


Fig. 4.— Rényi- α and KL divergence estimates ($\hat{D}_{R\alpha}$ and \hat{D}_{KL} ; **green**) between the likelihood distribution and the Section 4.2 ICA likelihood estimate for the B2017 P_ℓ (top) and S2017 ζ (bottom) analyses. We include the divergence estimates from Figure 1 for comparison. The ICA likelihood significantly improves the divergence discrepancy for both the P_ℓ and ζ analyses. For ζ , the improvement of the ICA likelihood over the pseudo-likelihood is more modest than our GMM estimate from Section 4.1. However, for P_ℓ , where the GMM method struggled, our ICA likelihood provides a significant improvement.

to increase the size of their observable data vector. However, as the divergence estimation framework we present makes it easy to test the accuracy of different methods, a hard choice is not necessary and multiple methods can easily be tested to construct the best estimate of the likelihood distribution for each specific analysis. Based on the performances of the GMM and ICA methods, in the following sections we use the ICA method for the [B2017](#) analysis and the GMM method for the [S2017](#) analysis.

5. Impact on Parameter Inference

To derive the posterior distribution of their model parameters, both [B2017](#) and [S2017](#) use the standard Monte Carlo Markov Chain (MCMC) approach with the Gaussian pseudo-likelihood. The [B2017](#) analysis includes 11 parameters,

$$\left\{ f\sigma_8, \alpha_{\parallel}, \alpha_{\perp}, b_1^{\text{NGC}}\sigma_8, b_1^{\text{SGC}}\sigma_8, b_2^{\text{NGC}}\sigma_8, b_2^{\text{SGC}}\sigma_8, \sigma_v^{\text{NGC}}, \sigma_v^{\text{SGC}}, N^{\text{NGC}}, \text{ and } N^{\text{SGC}} \right\},$$

while the [S2017](#) analysis includes 5 parameters,

$$\left\{ \log M_{\min}, \sigma_{\log M}, \log M_0, \log M_1, \text{ and } \alpha \right\}.$$

Using the improved likelihood estimates of Sections 4.1 and 4.2, we can now better estimate the true posterior distributions of these parameters and quantify the impact of likelihood non-Gaussianity on parameter constraints. The most straightforward approach to do this would be to use the likelihood estimates to compute MCMC samples from scratch. While this is relatively doable for the [B2017](#) analysis, for [S2017](#) this is *significantly* more involved. Rather than a perturbation theory based model from [B2017](#), the [S2017](#) model is a forward model, same as their mocks (Section 2.2). Rerunning the MCMC samples would involve evaluating their computationally costly forward model $> 10^5$ times.

Without having to re-run the MCMC chains, we instead use importance sampling to derive the new posteriors from the original chains (see [Wasserman 2004](#), for details on importance sampling). The *target* distribution we want is the new posterior. To sample this distribution, we sample the original posterior as the *proposal* distribution with importance weights, which in our case is the ratio of our likelihood estimates over the pseudo-likelihood. If we let $P(\mathbf{x}|\boldsymbol{\theta})$ be the original pseudo-likelihood and $P'(\mathbf{x}|\boldsymbol{\theta})$ be our “new” likelihood, then the new marginal likelihood can be calculated through importance sampling:

$$P'(\mathbf{x}|\theta_1) = \int P'(\mathbf{x}|\boldsymbol{\theta}) d\theta_2 \dots d\theta_m = \int \frac{P'(\mathbf{x}|\boldsymbol{\theta})}{P(\mathbf{x}|\boldsymbol{\theta})} P(\mathbf{x}|\boldsymbol{\theta}) d\theta_2 \dots d\theta_m \quad (19)$$

Through Monte Carlo integration, this becomes

$$P'(\mathbf{x}|\theta_1) \approx \sum_{\boldsymbol{\theta}^{(i)} \in S} \frac{P'(\mathbf{x}|\boldsymbol{\theta}^{(i)})}{P(\mathbf{x}|\boldsymbol{\theta}^{(i)})}. \quad (20)$$

where S is the sample drawn from $P(\mathbf{x}|\boldsymbol{\theta})$. In our case S is just the original MCMC chain. The only calculation required is the importance weights in Eq. 20, $P'(\mathbf{x}|\boldsymbol{\theta}^{(i)})/P(\mathbf{x}|\boldsymbol{\theta}^{(i)})$ for each sample $\boldsymbol{\theta}^{(i)}$ of the original MCMC chain. For B2017, $P(\mathbf{x}|\boldsymbol{\theta}^{(i)})$ is the ICA likelihood; for S2017, $P(\mathbf{x}|\boldsymbol{\theta}^{(i)})$ is the GMM likelihood.

We present in Figure 5 the resulting posterior distributions using the non-Gaussian ICA likelihood for the $\{f\sigma_8, \alpha_{\parallel}, \alpha_{\perp}, b_1^{\text{NGC}}\sigma_8, b_1^{\text{SGC}}\sigma_8, b_2^{\text{NGC}}\sigma_8, b_2^{\text{SGC}}\sigma_8, \}$ parameters in the B2017 P_{ℓ} analysis (orange). We include the original B2017 posteriors for comparison in blue. On the bottom of each panel, we also include box plots marking the confidence intervals of the updated and original posteriors. The boxes and “whiskers” represent the 68% and 95% confidence intervals, respectively. The median and 68% confidence intervals of the posteriors are listed in Table 1. $f\sigma_8$ and $b_2^{\text{SGC}}\sigma_8$ are the main parameters with noticeable change in their posteriors. The posterior of $b_2^{\text{SGC}}\sigma_8$ broadens from $0.476_{-1.175}^{+1.262}$ to $0.422_{-1.377}^{+1.517}$ once likelihood non-Gaussianity is incorporated. Meanwhile, the $f\sigma_8$ posterior shifts from $0.478_{-0.049}^{+0.053}$ to $0.456_{-0.049}^{+0.059}$, which corresponds to a shift of 0.44σ . The other parameter constraints, however, remain largely unaffected by likelihood non-Gaussianity.

Focusing on the main cosmological parameters $f\sigma_8$, α_{\parallel} , and α_{\perp} , we present their joint posterior distributions in Figure 6. The contours mark the 68% and 95% confidence intervals of the posteriors. The shift in the $f\sigma_8$ distribution is reflected in the $(f\sigma_8, \alpha_{\parallel})$ and $(\alpha_{\perp}, f\sigma_8)$ contours (left and middle panels respectively). The $(\alpha_{\parallel}, \alpha_{\perp})$ distribution (right), however, show nearly no change from the non-Gaussian likelihood. Despite its impact on $f\sigma_8$ and $b_2^{\text{SGC}}\sigma_8$, overall, likelihood non-Gaussianity does *not* significantly impact the parameter constraints of the P_{ℓ} analysis. $b_2^{\text{SGC}}\sigma_8$ is a poorly constrained nuisance parameter and although using the pseudo-likelihood biases $f\sigma_8$, the impact relative to its uncertainty is small — less than 0.5σ . The fact that the P_{ℓ} analysis is largely unaffected by likelihood non-Gaussianity is consistent with the divergences in Figure 1, which found relatively small discrepancies between the likelihood and pseudo-likelihood. It also illustrates the remarkable effectiveness of the Central Limit Theorem.

Next in Figure 7, we present the posterior distributions calculated using the non-Gaussian GMM likelihood for the HOD parameters in the S2017 ζ analysis (orange). We include the posteriors calculated using the pseudo-likelihood for comparison in blue. The box plots on the bottom of each plot mark the 68% and 95% confidence intervals of the posteriors. In the dotted lines, we plot the original S2017 posteriors, which differ slightly from the blue distribution. This difference is caused by the difference in the covariance matrix we use in the pseudo-likelihood (see Section 2.3). The difference, however, is negligible.

Besides the poorly constrained parameters $\sigma_{\log M}$ and $\log M_0$, likelihood non-Gaussianity significantly impacts the posterior distributions of the HOD parameters. Each of the parameter constraints for $\log M_{\min}$, $\log M_1$, and α , are significantly broader and also shifted compared to the pseudo-likelihood constraints (see Table 1 for details). The impact of likeli-

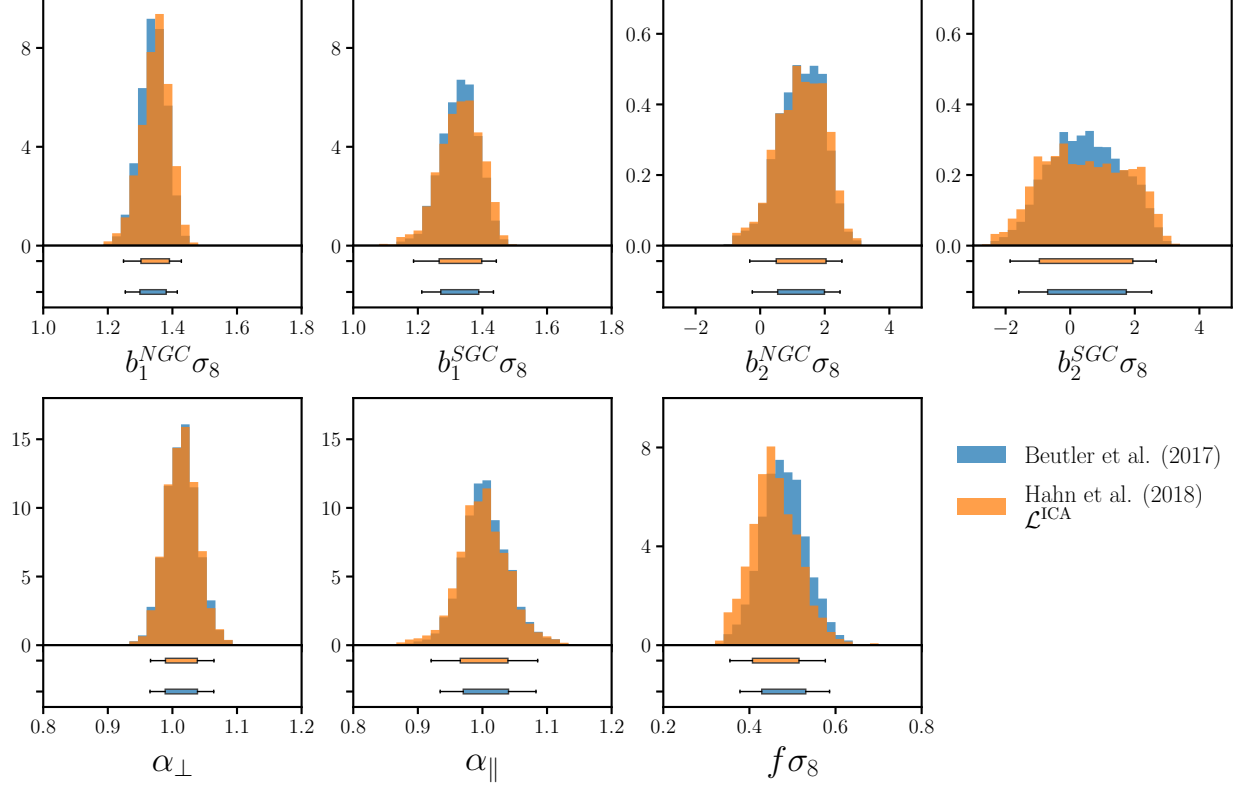


Fig. 5.— The posterior distribution for $\{f\sigma_8, \alpha_{\parallel}, \alpha_{\perp}, b_1^{\text{NGC}}\sigma_8, b_1^{\text{SGC}}\sigma_8, b_2^{\text{NGC}}\sigma_8, b_2^{\text{SGC}}\sigma_8, \}$ in the B2017 P_{ℓ} analysis using the non-Gaussian ICA likelihood (orange). We include in blue the original B2017 posteriors for comparison. On the bottom of each panel we include box plots that mark the 68% and 95% confidence intervals of the posterior. The discrepancy between the posteriors is most evident for the parameters $f\sigma_8$ and $b_2^{\text{SGC}}\sigma_8$. Hence, using the pseudo-likelihood in the P_{ℓ} analysis biases the posteriors of these parameters. Overall, however, likelihood non-Gaussianity does *not* have a significant impact on the parameter constraints of the P_{ℓ} analysis.

hood non-Gaussianity is further emphasized in the joint posterior distributions in Figure 8. The $\log M_{\min}$ versus $\sigma_{\log M}$ and $\log M_{\min}$ versus α contours are both shifted and broadened compared to the $\mathcal{L}^{\text{pseudo}}$ posterior. Figures 7 and 8 reveal that *using the Gaussian pseudo-likelihood significantly underestimates the uncertainty and biases the HOD parameter constraints of the S2017 ζ analysis.*

The contrast between the pseudo-likelihood posteriors and our posteriors in Figures 7 and 8 reflect the divergences in Figure 1, which revealed significant discrepancy between the ζ likelihood and the pseudo-likelihood. These divergences and posteriors are consistent with the expectation that the true ζ likelihood distribution is likely Poisson. Although we expect the likelihood to be similar to the observed cluster count likelihood, the complicated connection between FoF groups and the underlying matter overdensity makes writing down the exact ζ likelihood function tremendously difficult. Nonetheless, the GMM likelihood estimation method we present provides an accurate estimate of the non-Gaussian likelihood.

The posteriors of the S2017 ζ analysis, highlights the importance of accounting for likelihood non-Gaussianity in parameter inference of LSS studies. One of the main results of the S2017 HOD analysis is that the $\Lambda\text{CDM} + \text{HOD}$ model can successful fit either $\zeta(N)$ or the project two-point correlation function $w_p(r_p)$, separately but struggles to jointly fit both (see Figure 10). This tension suggests that the ‘vanilla’ HOD model is insufficiently flexible in describing the galaxy-halo connection. Likelihood non-Gaussianity, however, impacts this result. Once the non-Gaussianity is included in the analysis, the posteriors are broadened and shifted towards relaxing the tensions. We examine the effect of likelihood non-Gaussianity for HOD parameter constraints in more detail in Hahn et al. (in prep.).

Even for the P_ℓ analysis, the impact of likelihood non-Gaussianity on the parameter constraints cannot be easily dismissed as we demand increasingly more precise constraints from future experiments. Using the pseudo-likelihood biases the $f\sigma_8$ constraints by $\sim 0.5\%$. Meanwhile, the Dark Energy Spectroscopic Instrument (DESI; ?), for instance, seeks to constrain $f\sigma_8$ to within a percent⁴. The future, however, is encouraging in this regard. The next surveys will expand the cosmic volumes probed by galaxies and therefore increase the number of modes on all scales. Even as they seek to extend the k range of analyses, thanks to the Central Limit Theorem, we consequently expect likelihood non-Gaussianity to have a smaller effect. For higher order statistics, however, likelihood non-Gaussianity will still have a significant effect. After all, for a given survey, Scoccimarro (2000) found that the reduced bispectrum likelihood is significantly more non-Gaussian than the powerspectrum likelihood. Fortunately the methods we present in this paper can easily be extended to other observables and analyses.

⁴DESI Final Design Report: <http://desi.lbl.gov/wp-content/uploads/2014/04/fdr-science-biblatex.pdf>

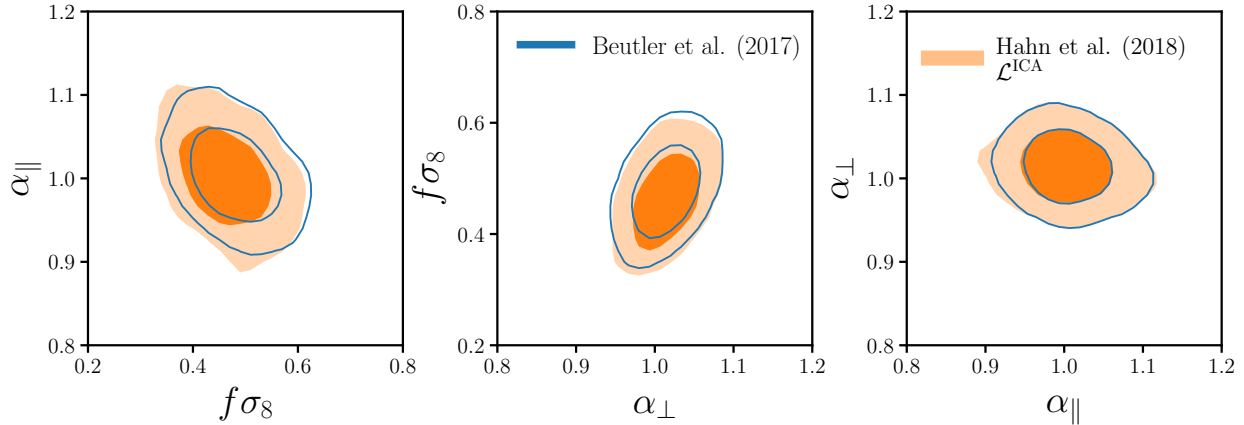


Fig. 6.— Joint posterior distributions of $f\sigma_8$, α_{\parallel} , and α_{\perp} in the B2017 P_{ℓ} analysis, compute using the non-Gaussian ICA likelihood (orange). We include, in blue, the original B2017 posteriors for comparison. The contours in the left and middle panels reflect the shift in $f\sigma_8$ caused by likelihood non-Gaussianity. Otherwise, the contours illustrate that likelihood non-Gaussianity has little impact on the cosmological parameters for the P_{ℓ} analysis.

Table 1: Impact of likelihood non-Gaussianity on the posterior parameter constraints of B2017 and S2017

B2017 P_ℓ analysis							
	$f\sigma_8$	α_\parallel	α_\perp	$b_1^{\text{NGC}}\sigma_8$	$b_1^{\text{SGC}}\sigma_8$	$b_2^{\text{NGC}}\sigma_8$	$b_2^{\text{SGC}}\sigma_8$
B2017	0.478	α_\parallel	α_\perp	$b_1^{\text{NGC}}\sigma_8$	$b_1^{\text{SGC}}\sigma_8$	$b_2^{\text{NGC}}\sigma_8$	$b_2^{\text{SGC}}\sigma_8$
non-Gaussian							
\mathcal{L}_{ICA}	0.478	α_\parallel	α_\perp	$b_1^{\text{NGC}}\sigma_8$	$b_1^{\text{SGC}}\sigma_8$	$b_2^{\text{NGC}}\sigma_8$	$b_2^{\text{SGC}}\sigma_8$
S2017 ζ analysis							

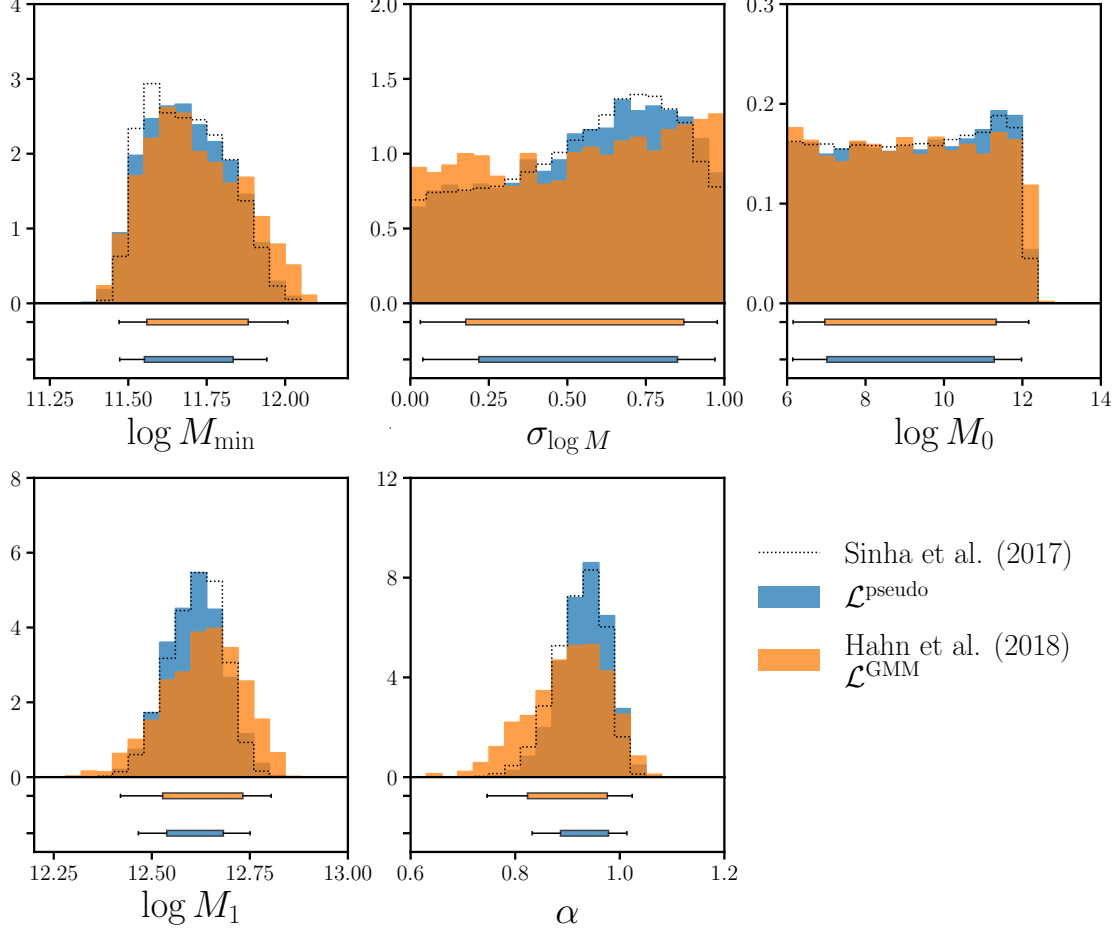


Fig. 7.— The posterior distribution for HOD parameters $\log M_{\min}$, $\sigma_{\log M}$, $\log M_0$, $\log M_1$, and α in the S2017 ζ analysis using the non-Gaussian GMM likelihood (orange). We include in blue the posteriors calculated from the pseudo-likelihood for comparison. We also include the original S2017 posterior (dotted; see text for details). On the bottom of each panel we include box plots that mark the 68% and 95% confidence intervals of the posterior. Besides the poorly constrained parameters $\sigma_{\log M}$ and $\log M_0$, the posteriors of $\log M_{\min}$, $\log M_1$, and α , are significantly broader and shifted compared to the pseudo-likelihood constraints. Likelihood non-Gaussianity significantly impacts the parameter constraints of the *zeta* analysis. Therefore using the pseudo-likelihood underestimates the uncertainty and biases the HOD parameter constraints.

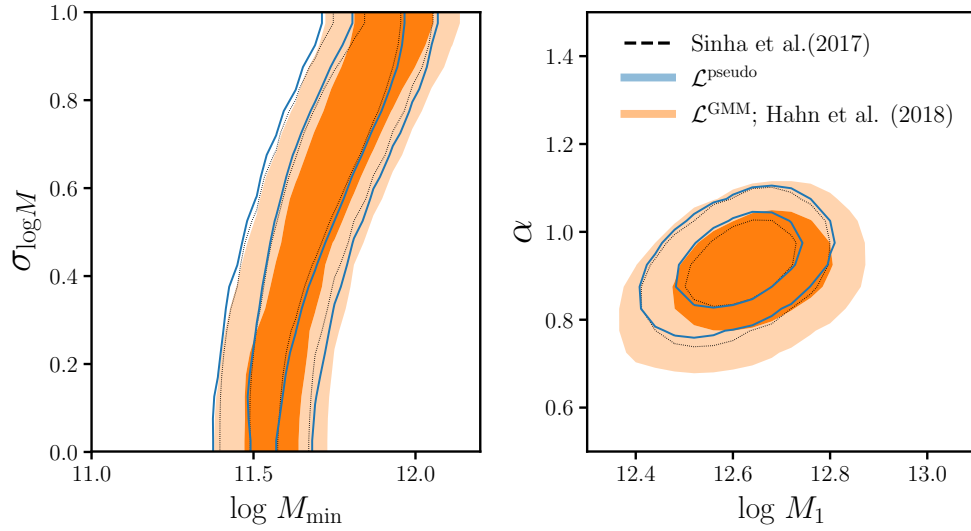


Fig. 8.— Joint posterior distributions of select HOD parameters in the [S2017](#) ζ analysis, compute using the non-Gaussian GMM likelihood (orange). We include, in blue, the posteriors computed using the pseudo-likelihood; we also include the original [S2017](#) posterior (dotted; see text for details). The contours confirm that that *due to likelihood non-Gaussianity, posteriors from the pseudo-likelihood underestimate the uncertainties and significantly biases the parameter constraints of the S2017 analysis.*

6. Summary and Discussion

Standard present day LSS analyses makes a major assumption in their parameter inference — the likelihood has a Gaussian functional-form. Although this assumption is motivated by the Central Limit Theorem, in detail this assumption cannot be true. In this paper, we investigate the impact of this assumption on two recent LSS analyses: the B2017 powerspectrum multipole ($\ell = 0, 2$, and 4) analysis and the S2017 group multiplicity function analysis. We combine mock catalogs, originally constructed for covariance matrix estimation in these analyses, with non-parametric divergence estimators to measure the divergences between the P_ℓ and ζ likelihoods and the Gaussian pseudo-likelihoods from B2017 and S2017. For both the P_ℓ and ζ likelihoods, the divergences reveal significant likelihood non-Gaussianity. For the P_ℓ likelihood, large scales (low k) and the hexadecapole contribute most to the relatively small non-Gaussianity. Meanwhile, for the ζ likelihood, the high richness end of ζ contribute most to the non-Gaussianity.

From the same mock catalogs of B2017 and S2017, we use non-parametric density estimation to construct estimates of the likelihood distribution that better approximates the true non-Gaussian P_ℓ and ζ likelihoods. For the ζ likelihood, the direct method of estimating the likelihood distribution with the mocks and Gaussian mixture density estimation results in an accurate estimate. For the B2017 P_ℓ analysis, which has fewer mocks and a higher dimensional likelihood, we use Independent Component Analysis to transform the likelihood distribution into statistically independent components. By estimating the one-dimensional distribution of these independent components, we derive an estimate of the high-dimensional likelihood distribution. The divergence between these two likelihood estimates and the P_ℓ and ζ likelihoods demonstrate that we derive *more accurate* estimates of the true likelihoods than the pseudo-likelihoods.

Finally, using the P_ℓ and ζ likelihood estimates and importance sampling, we derive posterior parameter constraint for the B2017 and S2017 analyses. Since our likelihood estimates are closer to the true likelihood, they allow us to derive more accurate posterior probability distributions than with Gaussian pseudo-likelihoods. By comparing our posteriors to the parameter constraints from B2017 and S2017, we find that likelihood non-Gaussianity does not significantly impact the P_ℓ analysis of B2017. Among the non-nuisance parameters, only $f\sigma_8$ is impacted by 0.44σ . Meanwhile for the S2017 ζ analysis, likelihood non-Gaussianity significantly impacts the posterior distributions of the HOD parameter. Using the pseudo-likelihood significantly underestimates the width of the $\log M_{\min}$, $\log M_1$, and α posteriors. It also significantly biases their constraints. In fact, accounting for likelihood non-Gaussianity, significantly eases the tension between the ζ and $w_p(r_p)$ constraints found in S2017. Our comparisons of the posteriors ultimately highlight the significance of likelihood non-Gaussianity in parameter inference of LSS studies.

Based on our results, P_ℓ analyses using future surveys (*e.g.* DESI) will not be significantly

impacted by likelihood non-Gaussianity. While these analyses seek to extend the k ranges probed, future surveys will also expand the cosmic volumes probed by galaxies and increase the number of modes on all scales. We therefore expect Central Limit Theorem to reduce the impact of likelihood non-Gaussianity. Likewise, we expect future surveys to also reduce the impact of likelihood non-Gaussianity on ζ analysis with the same multiplicity range, since larger cosmic volumes will probe more high multiplicity groups. For a wider multiplicity range, however, likelihood non-Gaussianity may still be a significant effect. For higher order statistics such as the galaxy bispectrum or three-point function, even for future surveys, likelihood non-Gaussianity will likely be a significant effect to consider for parameter inference. Regardless of our expectation, for ever more precise parameter inference the Gaussian likelihood assumption must be extensively tested. The divergence and likelihood estimations we introduce in this paper provide a straightforward framework for testing and quantifying the impact of likelihood non-Gaussianity on the final parameter constraints.

Our likelihood estimation methods allow us to go beyond the pseudo-likelihood and derive more accurate estimates of the likelihood. With a similar motivation at addressing likelihoods that are non-Gaussian or difficult to write down, methods for likelihood-free inference such as Approximate Bayesian Computation (ABC; [Hahn et al. 2017b](#); [Kacprzak et al. 2017](#); [Alsing & Wandelt 2017](#)) have recently been introduced to LSS studies. Although as a likelihood-free inference method, ABC has the advantage of relaxing *any* assumption on the likelihood, even with smart sampling methods like Population Monte Carlo, it requires an expensive generative forward model to be computed far more times than the number of mocks required for covariance matrix estimation. Our methods (especially the ICA method) do not require any more mocks than those already constructed for accurate covariance matrix estimation. Therefore, the methods for likelihood estimation we present in this paper provide both accurate and practical methods for Bayesian parameter inference in LSS.

Acknowledgements

It’s a pleasure to thank Simone Ferraro, David W. Hogg, Emmaneul Schaan, Uroš Seljak, and Roman Scoccimarro for valuable discussions. **more acknowledgements** This project made use of the NASA Astrophysics Data System and open-source software Python, numpy, SciPy, matplotlib, and Scikit-learn.

REFERENCES

- Ade, P. a. R., Aghanim, N., Arnaud, M., et al. 2016, [Astronomy & Astrophysics](#), 594, A24
 Alam, S., Ata, M., Bailey, S., et al. 2017, [Monthly Notices of the Royal Astronomical Society](#), 470, 2617
 Alsing, J., & Wandelt, B. 2017, arXiv:1712.00012 [astro-ph], [arXiv:1712.00012 \[astro-ph\]](#)

- Arthur, D., & Vassilvitskii, S. 2007, in Proceedings of the Eighteenth Annual ACM-SIAM Symposium on Discrete Algorithms, SODA '07 (Philadelphia, PA, USA: Society for Industrial and Applied Mathematics), 1027
- Berlind, A. A., Frieman, J., Weinberg, D. H., et al. 2006, [The Astrophysical Journal Supplement Series](#), **167**, 1
- Beutler, F., Seo, H.-J., Saito, S., et al. 2017, [Monthly Notices of the Royal Astronomical Society](#), **466**, 2242
- Bianchi, D., Gil-Marín, H., Ruggeri, R., & Percival, W. J. 2015, [Monthly Notices of the Royal Astronomical Society](#), **453**, L11
- Bovy, J., Hogg, D. W., & Roweis, S. T. 2011, [The Annals of Applied Statistics](#), **5**, 1657
- Broderick, A. E., Fish, V. L., Doeleman, S. S., & Loeb, A. 2011, [The Astrophysical Journal](#), **735**, 110
- Cash, W. 1979, [The Astrophysical Journal](#), **228**, 939
- Collaboration, P., Ade, P. A. R., Aghanim, N., et al. 2014, [Astronomy & Astrophysics](#), **571**, A20
- Comon, P. 1994, [Signal Processing](#), **36**, 287
- Crocce, M., Pueblas, S., & Scoccimarro, R. 2006, [Monthly Notices of the Royal Astronomical Society](#), **373**, 369
- Davis, M., Efstathiou, G., Frenk, C. S., & White, S. D. M. 1985, [The Astrophysical Journal](#), **292**, 371
- Davison, A. C. 2008, Statistical Models (Cambridge Series in Statistical and Probabilistic Mathematics) (Cambridge University Press)
- Dempster, A. P., Laird, N. M., & Rubin, D. B. 1977, Journal of the Royal Statistical Society. Series B (Methodological), **39**, 1
- Eifler, T., Schneider, P., & Hartlap, J. 2009, [Astronomy and Astrophysics](#), **502**, 721
- Eisenstein, D. J., & Zaldarriaga, M. 2001, [The Astrophysical Journal](#), **546**, 2
- Feigelson, E. D., & Babu, G. J. 2012, Modern Statistical Methods for Astronomy
- Fraley, C., & Raftery, A. E. 1998, [The Computer Journal](#), **41**, 578
- Gardner, J. P., Connolly, A., & McBride, C. 2007, in Astronomical Data Analysis Software and Systems XVI, Vol. 376, 69
- Gaztañaga, E., & Scoccimarro, R. 2005, [Monthly Notices of the Royal Astronomical Society](#), **361**, 824
- Grieb, J. N., Sánchez, A. G., Salazar-Albornoz, S., et al. 2017, [Monthly Notices of the Royal Astronomical Society](#), **467**, 2085
- Guo, H., Zehavi, I., & Zheng, Z. 2012, [The Astrophysical Journal](#), **756**, 127
- Hahn, C., Scoccimarro, R., Blanton, M. R., Tinker, J. L., & Rodríguez-Torres, S. A. 2017a, [Monthly Notices of the Royal Astronomical Society](#), **467**, 1940
- Hahn, C., Vakili, M., Walsh, K., et al. 2017b, [Monthly Notices of the Royal Astronomical](#)

- [Society](#), 469, 2791
- Hand, N., Feng, Y., Beutler, F., et al. 2017a
- Hand, N., Li, Y., Slepian, Z., & Seljak, U. 2017b, [Journal of Cosmology and Astro-Particle Physics](#), 07, 002
- Hartlap, J., Schrabback, T., Simon, P., & Schneider, P. 2009, [Astronomy and Astrophysics](#), 504, 689
- Hastie, T., Tibshirani, R., & Friedman, J. 2009, *The Elements of Statistical Learning: Data Mining, Inference, and Prediction*, Second Edition (Springer Series in Statistics) (Springer)
- Hérault, J., & Ans, B. 1984, *Comptes Rendus de l’Académie des Sciences Paris, Série III, Life Sciences*, 299, 525
- Hogg, D. W., Bovy, J., & Lang, D. 2010, ArXiv e-prints, 1008, arXiv:1008.4686
- Hyvärinen, A. 1998, in *Advances in Neural Information Processing Systems 10*, ed. M. I. Jordan, M. J. Kearns, & S. A. Solla (MIT Press), 273
- Hyvarinen, A. 1999, [IEEE Transactions on Neural Networks](#), 10, 626
- . 2001, *Independent Component Analysis* (New York: J. Wiley)
- Hyvärinen, A., & Oja, E. 2000, *Neural Networks: The Official Journal of the International Neural Network Society*, 13, 411
- Kacprzak, T., Herbel, J., Amara, A., & Réfrégier, A. 2017, arXiv:1707.07498 [astro-ph], [arXiv:1707.07498 \[astro-ph\]](#)
- Kazin, E. A., Koda, J., Blake, C., et al. 2014, [Monthly Notices of the Royal Astronomical Society](#), 441, 3524
- Kitaura, F.-S., Gil-Marín, H., Scóccola, C. G., et al. 2015, [Monthly Notices of the Royal Astronomical Society](#), 450, 1836
- Kitaura, F.-S., & Heß, S. 2013, [Monthly Notices of the Royal Astronomical Society](#), 435, L78
- Kitaura, F.-S., Yepes, G., & Prada, F. 2014, [Monthly Notices of the Royal Astronomical Society](#), 439, L21
- Kitaura, F.-S., Rodríguez-Torres, S., Chuang, C.-H., et al. 2016, [Monthly Notices of the Royal Astronomical Society](#), 456, 4156
- Klypin, A., Yepes, G., Gottlöber, S., Prada, F., & Heß, S. 2016, [Monthly Notices of the Royal Astronomical Society](#), 457, 4340
- Krishnamurthy, A., Kandasamy, K., Poczos, B., & Wasserman, L. 2014, arXiv:1402.2966 [math, stat], [arXiv:1402.2966 \[math, stat\]](#)
- Kuhn, M. A., & Feigelson, E. D. 2017, arXiv:1711.11101 [astro-ph, stat], [arXiv:1711.11101 \[astro-ph, stat\]](#)
- Lee, K. J., Guillemot, L., Yue, Y. L., Kramer, M., & Champion, D. J. 2012, [Monthly Notices of the Royal Astronomical Society](#), 424, 2832

- Leroux, B. G. 1992, [The Annals of Statistics](#), 20, 1350
- Liddle, A. R. 2007, [Monthly Notices of the Royal Astronomical Society](#), 377, L74
- Lloyd, S. 1982, [IEEE Transactions on Information Theory](#), 28, 129
- McBride, C., Berlind, A., Scoccimarro, R., et al. 2009, in *Bulletin of the American Astronomical Society*, Vol. 213, 425.06
- McLachlan, G., & Peel, D. 2000, *Finite Mixture Models* (Wiley-Interscience)
- Mohammed, I., Seljak, U., & Vlah, Z. 2017, [Monthly Notices of the Royal Astronomical Society](#), 466, 780
- Neal, R. M., & Hinton, G. E. 1998, in [Learning in Graphical Models](#), NATO ASI Series (Springer, Dordrecht), 355
- Norberg, P., Baugh, C. M., Gaztañaga, E., & Croton, D. J. 2009, [Monthly Notices of the Royal Astronomical Society](#), 396, 19
- Ntampaka, M., Trac, H., Sutherland, D. J., et al. 2015, [The Astrophysical Journal](#), 803, 50
- . 2016, [The Astrophysical Journal](#), 831, 135
- Parkinson, D., Riemer-Sørensen, S., Blake, C., et al. 2012, [Physical Review D](#), 86, 103518
- Pinol, L., Cahn, R. N., Hand, N., Seljak, U., & White, M. 2017, [Journal of Cosmology and Astroparticle Physics](#), 2017, 008
- Póczos, B., Szabó, Z., & Schneider, J. 2011, in *2011 19th European Signal Processing Conference*, 1718
- Poczos, B., Xiong, L., & Schneider, J. 2012a, arXiv:1202.3758 [cs, stat], [arXiv:1202.3758 \[cs, stat\]](#)
- Poczos, B., Xiong, L., Sutherland, D., & Schneider, J. 2012b, *Machine Learning Department*
- Póczos, B., Xiong, L., Sutherland, D. J., & Schneider, J. 2012, in [2012 IEEE Conference on Computer Vision and Pattern Recognition](#), 2989
- Press, W. H., Teukolsky, S. A., Vetterling, W. T., & Flannery, B. P. 1992, *Numerical Recipes in C (2Nd Ed.): The Art of Scientific Computing* (New York, NY, USA: Cambridge University Press)
- Ravanbakhsh, S., Lanusse, F., Mandelbaum, R., Schneider, J., & Poczos, B. 2017, in *Thirty-First AAAI Conference on Artificial Intelligence*
- Rodríguez-Torres, S. A., Chuang, C.-H., Prada, F., et al. 2016, [Monthly Notices of the Royal Astronomical Society](#), 460, 1173
- Roeder, K., & Wasserman, L. 1997, [Journal of the American Statistical Association](#), 92, 894
- Ross, A. J., Beutler, F., Chuang, C.-H., et al. 2017, [Monthly Notices of the Royal Astronomical Society](#), 464, 1168
- Schwarz, G. 1978, [The Annals of Statistics](#), 6, 461
- Scoccimarro, R. 1998, [Monthly Notices of the Royal Astronomical Society](#), 299, 1097
- . 2000, [The Astrophysical Journal](#), 544, 597

- . 2015, [Physical Review D](#), **92**, [arXiv:1506.02729](#)
- Scott, D. W. 1992, *Multivariate Density Estimation: Theory, Practice, and Visualization* (Wiley)
- Sellentin, E., Jaffe, A. H., & Heavens, A. F. 2017, [arXiv:1709.03452 \[astro-ph, stat\]](#),
[arXiv:1709.03452 \[astro-ph, stat\]](#)
- Sinha, M., Berlind, A. A., McBride, C. K., et al. 2017, [arXiv:1708.04892 \[astro-ph\]](#),
[arXiv:1708.04892 \[astro-ph\]](#)
- Slepian, Z., Eisenstein, D. J., Brownstein, J. R., et al. 2017, [Monthly Notices of the Royal Astronomical Society](#), **469**, 1738
- Springel, V. 2005, [Monthly Notices of the Royal Astronomical Society](#), **364**, 1105
- Steele, R. J., & Raftery, A. E. 2010
- Taylor, E. N., Hopkins, A. M., Baldry, I. K., et al. 2015, [Monthly Notices of the Royal Astronomical Society](#), **446**, 2144
- Tinker, J. L., & et al. in preparation
- Vakili, M., & Hahn, C. H. 2016, [arXiv:1610.01991 \[astro-ph\]](#), [arXiv:1610.01991 \[astro-ph\]](#)
- Vargas-Magaña, M., Ho, S., Xu, X., et al. 2014, [Monthly Notices of the Royal Astronomical Society](#), **445**, 2
- Wang, Q., Sanjeev, K., & Sergio, V. 2009, *IEEE TRANSACTIONS ON INFORMATION THEORY*, **55**, 2392
- Wasserman, L. 2004, *All of Statistics: A Concise Course in Statistical Inference* (Springer Texts in Statistics) (Springer)
- Wilkinson, D. M., Maraston, C., Thomas, D., et al. 2015, [Monthly Notices of the Royal Astronomical Society](#), **449**, 328
- Wu, C. F. J. 1983, [The Annals of Statistics](#), **11**, 95
- Xu, X., Ho, S., Trac, H., et al. 2013, [The Astrophysical Journal](#), **772**, 147
- Zhao, C., Kitaura, F.-S., Chuang, C.-H., et al. 2015, [Monthly Notices of the Royal Astronomical Society](#), **451**, 4266
- Zheng, Z., Coil, A. L., & Zehavi, I. 2007, [The Astrophysical Journal](#), **667**, 760